AIP | Review of Scientific Instruments

DELICIOUS III: A multipurpose double imaging particle coincidence spectrometer for gas phase vacuum ultraviolet photodynamics studies

G. A. Garcia, B. K. Cunha de Miranda, M. Tia, S. Daly, and L. Nahon

Citation: Rev. Sci. Instrum. **84**, 053112 (2013); doi: 10.1063/1.4807751
View online: http://dx.doi.org/10.1063/1.4807751
View Table of Contents: http://rsi.aip.org/resource/1/RSINAK/v84/i5
Published by the American Institute of Physics.

Additional information on Rev. Sci. Instrum.

Journal Homepage: http://rsi.aip.org
Journal Information: http://rsi.aip.org/about/about_the_journal
Top downloads: http://rsi.aip.org/features/most_downloaded
Information for Authors: http://rsi.aip.org/authors

ADVERTISEMENT

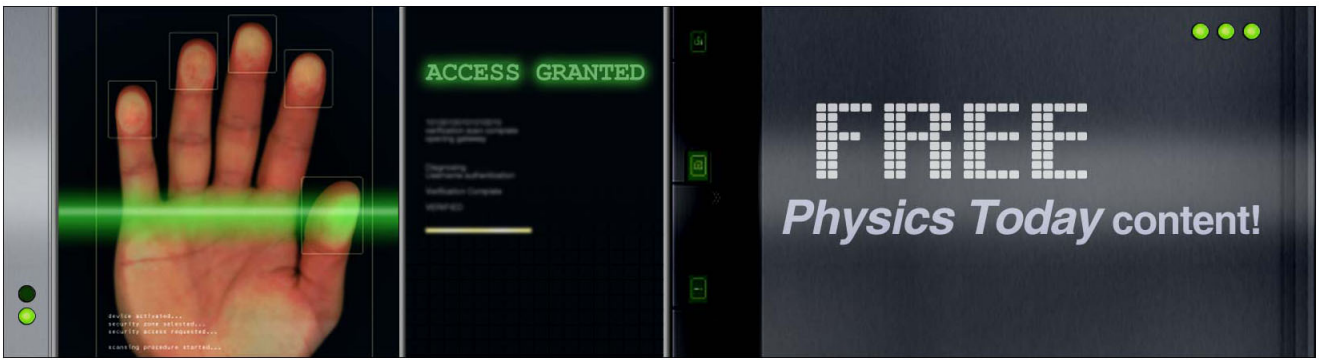

Downloaded 30 May 2013 to 195.221.0.6. This article is copyrighted as indicated in the abstract. Reuse of AIP content is subject to the terms at: http://rsi.aip.org/about/rights_and_permissions

DELICIOUS III: A multipurpose double imaging particle coincidence spectrometer for gas phase vacuum ultraviolet photodynamics studies

G. A. Garcia,[a] B. K. Cunha de Miranda, M. Tia, S. Daly, and L. Nahon
Synchrotron SOLEIL, L'Orme des Merisiers, St. Aubin BP 48, 91192 Gif sur Yvette, France

(Received 19 April 2013; accepted 12 May 2013; published online 30 May 2013)

We present a versatile double imaging particle coincidence spectrometer operating in fully continuous mode, named DELICIOUS III, which combines a velocity map imaging device and a modified Wiley-McLaren time of flight momentum imaging analyzer for photoelectrons and photoions, respectively. The spectrometer is installed in a permanent endstation on the DESIRS vacuum ultraviolet (VUV) beamline at the French National Synchrotron Radiation Facility SOLEIL, and is dedicated to gas phase VUV spectroscopy, photoionization, and molecular dynamics studies. DELICIOUS III is capable of recording mass-selected threshold photoelectron photoion coincidence spectra with a sub-meV resolution, and the addition of a magnifying lens inside the electron drift tube provides a sizeable improvement of the electron threshold/ion mass resolution compromise. In fast electron mode the ultimate kinetic energy resolution has been measured at $\Delta E/E = 4\%$. The ion spectrometer offers a mass resolution—full separation of adjacent masses—of 250 amu for moderate extraction fields and the addition of an electrostatic lens in the second acceleration region allows measuring the full 3D velocity vector for a given mass with an ultimate energy resolution of $\Delta E/E = 15\%$, without sacrificing the mass resolution. Hence, photoelectron images are correlated both to the mass and to the ion kinetic energy and recoil direction, to access the electron spectroscopy of size-selected species, to study the photodissociation processes of state-selected cations in detail, or to measure in certain cases photoelectron angular distributions in the ion recoil frame. The performances of DELICIOUS III are explored through several examples including the photoionization of N_2, NO, and CF_3. © *2013 AIP Publishing LLC*. [http://dx.doi.org/10.1063/1.4807751]

I. INTRODUCTION

Imaging charged particles spectrometers providing a dual angular and radial momentum information have become, for the last decades, a widely used tool in chemical[1] and photoionization dynamics,[2] for laser and synchrotron based studies. This is especially the case of velocity map imaging (VMI) spectrometers[3] because of their particle momentum resolution advantages over the original imaging devices. A few years ago we expanded the well-known capabilities of the VMI by adding a Wiley-McLaren (WM) type Time of Flight (TOF) ion analyzer to operate in a photoelectron/photoion coincidence (PEPICO) scheme.[4] The apparatus, called DELICIOUS II, has been in operation since early 2009 in one of the permanent endstations—the molecular beam chamber SAPHIRS—of the Vacuum UltraViolet (VUV) beamline DESIRS,[5] located at the French National Synchrotron Radiation (SR) Facility SOLEIL. In view of the broad scientific case of the beamline, the spectrometer was conceived for versatility and thus had to be able to operate in continuous mode, the natural time-structure of SR, and detect fast as well as threshold photoelectrons in coincidence with ions for studying VUV photoionization dynamics, along with the spectroscopy and fragmentation of state-selected cations, on a wide range of mass-selected targets, from diatomics to biomolecules, and from molecular complexes to large clusters. The spectrometer has now been successfully used by a large number of in-house and external research groups, accounting for an average of 40% of all the beamline projects.

In parallel[6] and later on,[7,8] other designs at synchrotron facilities have added TOF ion mass spectrometry to the VMI principle and benefited from the advantages of coincidence operation.

In spite of the remarkable performance of DELICIOUS II, there are several aspects that could still be improved or added in order to broaden the scientific opportunities offered to the DESIRS beamline users' community, notably:

1. *Improvement of the ion mass resolution*. This point is critical for the study of medium to relatively large sized molecules, such as biomolecules (amino acids, nucleotides, small peptides, etc.) or clusters, where the moderate resolution of DELICIOUS II (∼100 amu) might be an unwelcome limitation, especially in dissociative ionization leading to small mass differences, such as hydrogen loss.
2. *Ion kinetic energy measurement and correlation to the coincident electron energy*. This point constitutes the main disadvantage of DELICIOUS II and was the driving force of the upgrade. The ion kinetic energy could already be measured on the VMI by inverting the electrodes' potential and detecting the electrons on the WM side. Although the inversion was somewhat cumbersome, mass-selected photoion imaging was successfully applied to measure the translational energy of a given mass, and determine whether it came from a direct, or dissociative ionization event.[9,10] In addition, this mode

[a]Author to whom correspondence should be addressed. Electronic mail: gustavo.garcia@synchrotron-soleil.fr

 © 2013 AIP Publishing LLC

Downloaded 30 May 2013 to 195.221.0.6. This article is copyrighted as indicated in the abstract. Reuse of AIP content is subject to the terms at: http://rsi.aip.org/about/rights_and_permissions

of operation was routinely used for the alignment and optimization of the molecular beam. However, the electron kinetic energy information was lost, and with that, a number of interesting applications such as:

- *Detailed thermochemical information on the cation fragmentation such as activation energies*. In this case the selection of the electron energy defines a specific internal state of the parent cation—via, for instance, threshold photoelectron photoion coincidence (TPEPICO) spectroscopy—while the coincident ion kinetic energy of the fragment provides information on the activation energy. The ion kinetic energy can also help disentangle different fragmentation pathways leading to the same fragment mass, but with different internal energy of the neutral or/and the cation fragments.
- *Photoelectron spectroscopy of size-selected targets*. Mass-selection does not lead necessarily to size-selection, since the mass can either be a parent ion, or a fragment from dissociative ionization. This is especially true in complicated mixtures such as cluster production where there are many different nascent neutral parent clusters in the molecular beam that can form lower order clusters in cascading dissociative ionization processes. Selecting only the ions without an excess thermal energy leads, however, to size-selection and allows the photoelectron spectroscopy of pure nascent species to be recorded. Other examples of complex mixtures where the kinetic energy correlation would be desirable involve radical production, where the precursor might fragment upon ionization to give the same mass as the radical,[10,11] or in general, complex gas phase reactions where it is important to know whether a given mass corresponds to the species being ionized.

3. *Improvement of the electron bandwidth*. For photoionization dynamics, where experimental observables such as partial cross-sections and photoelectron angular parameters, depend on the particle's kinetic energy, it is interesting to increase the bandwidth to allow comparisons with theoretical models to be made over a wider range, while keeping reasonable voltages on the spectrometer's plates and detectors.
4. *Relax the compromise between electron and ion mass resolutions in TPEPICO mode*. About half the experimental projects utilizing DELICIOUS II were focused on recording the cation spectroscopy with the TPEPICO mode of operation. However, in a WM spectrometer, the mass resolution improves proportionally to the square root of the extraction field,[12] while the electron threshold bandwidth ($\Delta\varepsilon$) worsens proportionally.[4] Thus, decreasing the extraction field to reach the ultimate electron resolution is not compatible with the study of medium/large molecules. In addition, the transmission of large molecules might be dramatically decreased, due to their velocity along the molecular beam, for low extraction fields. Deflectors can compensate this longitudinal energy but at the expense of mass resolution.

Of course, the above requirements need to be compatible with a synchrotron multi-user shared endstation, notably being versatile and able to work in the natural synchrotron's CW mode of operation, in addition to being as reliable and user friendly as possible, in order to eliminate the need for a setup time between projects. Section II A describes the compromises and choices made in conceiving the spectrometer, and how it compares with existing designs featuring double particle imaging.

II. CONCEPTION

A. Design considerations

Double particle imaging devices[13] require the measurement of the electron's TOF to reconstruct the photoelectron's Newton sphere[14] and as such, they are only compatible with short-pulsed light sources, where the electron TOF can be precisely measured with respect to the photons. Since in modern synchrotron facilities the amount of beamtime in the few bunch mode (pulsed-operation) is extremely limited, photoelectron spectrometers that rely on the electron TOF coordinate[15,16] are not a viable option for a user-oriented set-up. The next logical option, a double VMI, deserves more consideration. Indeed, such a design has been elegantly achieved by Janssen *et al.*[17,18] and recently refined to utilize a single VMI analyzer to detect both electrons and ions in coincidence.[19] However, numerical raytracing simulations show that the presence of an open, gridless repeller, necessary for the double VMI design, significantly reduces the particle's energy resolution. Janssen *et al*. overcome this problem by virtually "closing" the repeller through the application of pulsed voltages on the electrodes located behind, by the insertion of an extra electrode between the extractor and the drift tube, and by using fs-laser pulses to temporally slice the photoelectron's Newton sphere. Apparatus in operation at the VUV beamlines at the SLS (Villegen)[20] and NSRL (Heifei)[7] synchrotrons are also based upon a double VMI design with the inclusion of the extra electrode and both predicted a theoretical energy resolution of 2.5%. While the SLS group provides no quantitative information on the mass resolution, the NSRL group reported a high mass resolving power of $M/\Delta M = 900$ due to their long ion flight path (38 cm). Note that at NSRL, the presence of a CCD camera instead of a delay-line anode in the ion side necessitates pulsing the ion Micro-Channel Plates (MCPs) to obtain mass-selected ion images, losing the multiplex advantage. A double velocity imaging apparatus has also been in operation at the Photon Factory in Japan for a number of years,[21] and has been optimized for inner shell vector correlation studies where fast Auger electrons need to be detected alongside the photoelectrons, in coincidence with small ions so that mass resolution is not an issue.

Because pulsed operation needs complicated data processing and analysis schemes[22] to remove the ever-present false coincidences, and since we wanted to improve the cation time focusing to increase the mass resolution while measuring

Downloaded 30 May 2013 to 195.221.0.6. This article is copyrighted as indicated in the abstract. Reuse of AIP content is subject to the terms at: http://rsi.aip.org/about/rights_and_permissions

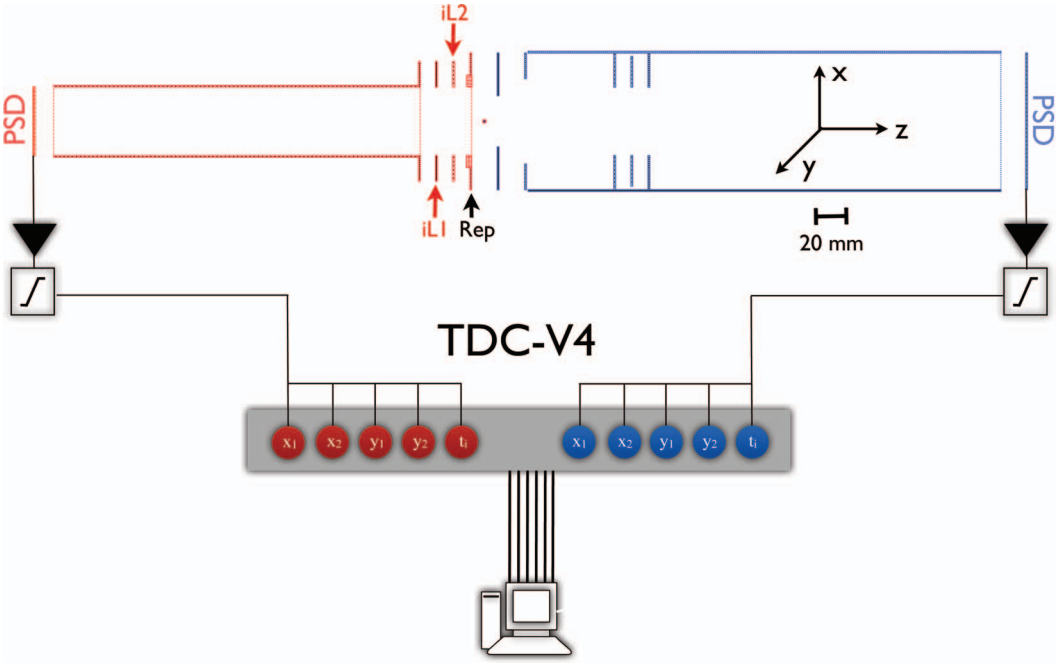

FIG. 1. Scaled down schematic of the DELICIOUS III spectrometer (red (respectively, blue) corresponds to the ion side (respectively, electron)) and the data acquisition chain. The total length of the spectrometer measured between the two PSDs is 579 mm. Dashed lines represent meshes.

the ion momentum vector event by event without the need of image inversion, we chose to implement a modified CW WM imaging spectrometer on the ion side instead of another VMI. Indeed the event by event measurement is necessary to correlate photoelectron images with a given ion 3D momentum when the electron TOF is not available, and a WM spectrometer provides the natural time focusing.

A schematic of the final double imaging PEPICO design, hereafter named DELICIOUS III, is presented in Figure 1, and it meets all the requirements outlined in Sec. I. The design has been optimized using a custom numerical simulation code to solve the Laplace equation. The ion side now includes a 40 mm custom-made position sensitive detector (PSD) based on a delay-line anode,[23] placed at the end of a WM spectrometer with two acceleration regions. Inside the second acceleration region, two gridless electrodes (iL2 and iL1), similar to what has already been implemented in other imaging devices,[24] provide the space focusing onto the detector plane, in addition to the inherent time focusing of the WM concept. The electrostatic lens created by iL2 and iL1 is not located at the center of the ionization region, therefore the spatial resolution will be somewhat degraded with respect to a VMI (see Sec. III B), but is balanced by a better mass/time resolution. Two deflectors along the molecular beam's direction have also been added to compensate for the beam's velocity for the study of heavy species.

On the electron side, the PSD's diameter has been multiplied by two (from 40 to 80 mm) with the addition of a commercial Roentdek DLD80 delay-line anode, while the drift tube has been slightly elongated, leading to a nearly four-fold increase of the kinetic energy bandwidth. Inside the electron drift tube, a divergent thin lens has been inserted to magnify slow photoelectron images, i.e., to discriminate more efficiently the fast electrons for a given extraction field. Because the spectrometer is also designed to map out fast electrons, the minimum aperture of the divergent lens is limited as compared to the design proposed by Offerhaus *et al.*,[25] therefore restricting the magnification.

On both VMI and WM sides, the kinetic energy resolution can be increased, at the expense of bandwidth, by merely lengthening the drift tubes. However, here we are constrained by the geometry of the SAPHIRS molecular beam chamber, so that the total length is not far from the maximum allowed. Furthermore, the maximum radius of the electrodes, which should be as large as possible to limit stray field penetration, needs to be balanced with the increasing distance from the nozzle to the interaction region, leading to a signal decrease with the square of this distance.

B. Signal and data acquisition

As shown in Figure 1, both ion and electron PSDs are based upon a four corner delay-line anode, which measures the particle's position via its arrival times on the four corners of the anode. The eight position signals plus two fast signals taken from the electron and ion MCPs are pre-amplified, discriminated, and fed into a custom-made Time to Digital Convertor (TDC), which constitutes the core of the data acquisition chain. The TDC has been conceived by the DTPI (Détection: Temps, Position et Image) platform, at the Institut de Sciences Moléculaires (Orsay, France), and it is constructed around the field programmable grid array Virtex-4, manufactured by Xilinx. The TDC is connected to the computer's PCI bus and operates with a 120 ps time coding step (although it can be reduced to 60 ps), and a double hit resolution, or dead time, lower than 2.5 ns per channel. We have

Downloaded 30 May 2013 to 195.221.0.6. This article is copyrighted as indicated in the abstract. Reuse of AIP content is subject to the terms at: http://rsi.aip.org/about/rights_and_permissions

experimentally measured a data flux of 14.5 Mstops/s, which in our case translates into 1.5 Mevents/s without any data loss.

The data acquisition program, written in C++ and embedded into the commercial data analysis and visualization program Igor Pro, writes the data flux directly to a remote server for off-line treatment, and also processes the events in real time according to the user commands in a multistart/ multistop (MS/MS) scheme. With respect to other coincidence schemes, the MS/MS scheme ensures a better signal-to-noise ratio and a more random spread of false coincidences over the temporal window, providing a better noise subtraction.[26] Both PSDs have been spatially calibrated (time-to-position, distortion) with a microscopy mask, and the relation between image radius and particle kinetic energy has been obtained using rare gases as calibrants.

III. MEASURED PERFORMANCES

In the following we provide a full description of the performances of DELICIOUS III.

A. Electron energy analysis

To characterize the performance of the VMI spectrometer, the first step is the kinetic energy calibration of the PSD detector in order to quantify the relation between kinetic energy and radial detector coordinate. The relation is given by the expression:

$$E = |q|V_{rep}R^2/C^2,$$

where q is the particle charge, V_{rep} is the repeller voltage, R is the radial detector coordinate, and C a calibration coefficient. To determine the C coefficient, we have recorded for a given repeller voltage, several photoelectron images from the Xe photoionization at different photon energies. By relating the kinetic energy of the Xe $(5p^{-1})$ $^2P_{3/2}$ and $^2P_{1/2}$ photoelectrons with the radial coordinate we obtained a value of C_{VMI} = 48.6 cm. This corresponds to an increase of the electron energy bandwidth by a factor of 3.6 as compared to the former spectrometer.[27]

The Xe images were also Abel inverted using the pBasex algorithm[28] to extract the resolution as the Full Width at Half Maximum (FWHM) of the Xe $(5p^{-1})$ PhotoElectron Spectra (PES) bands. The experimental electron resolution ($\Delta E/E$) as a function of the electron kinetic energy (KE) for a given fixed repeller is illustrated on Figure 2. A slight improvement of resolution is observed as compared to the precedent spectrometer[4] and we have actually reached an ultimate resolution of $\Delta E/E = 4\%$ at $\rho = 0.005$ (R = 3.4 cm) on N_2, where $\rho = E/V_{rep}$. Also plotted in Figure 2 alongside the experimental data is the calculated resolution curve obtained via numerical raytracing simulations assuming a cylindrical volume source of 6 mm length along the light's propagation axis, and 200 μm diameter, corresponding to the typical size of the light's spot at the focal point, when wide exit slits of the monochromator are used. There is a very good agreement for $\rho < 0.004$ (R < 3 cm), while for larger ρ, the curves exhibit small differences that can reach a factor of 1.5 with respect to the calculated values at the edge of the detector. The disagreement is most probably due to the off-axis aberrations that are expected to be more evident for trajectories far from the lens axis, i.e., for fast electrons, in accordance to Figure 2. Evidently, the main limiting factor in terms of energy resolution is the volume source, specifically the dimension along the SR axis, currently estimated at 6 mm. Thus a large improvement can be expected by the addition of a second skimmer to provide a narrower molecular beam at the spectrometer's center,[29] an upgrade that will be implemented in SAPHIRS in the short therm.

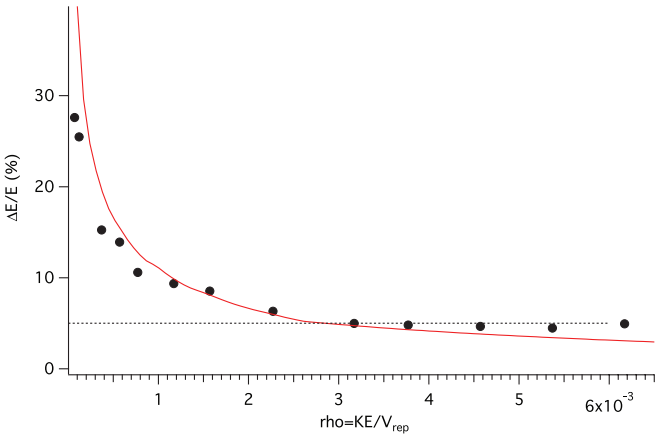

FIG. 2. Electron energy resolution $\Delta E/E$ as a function of the E/V_{rep} ratio. Black solid circles represent the experimental values obtained at different ionization energies for Xe at a fixed repeller of 1000 V. The red solid line corresponds to the simulated resolution assuming a cylindrical volume source of dimensions L = 6 mm and R = 100 μm. The horizontal dashed line at $\Delta E/E = 5\%$ is shown as a visual aid.

As previously documented,[4,6,30] the VMI can be used to record threshold electrons by measuring the counts on the center of the detector, and subtracting the hot electrons' contribution to this center obtained from an outer, or crown region. The advantages of measuring a threshold photoelectron spectrum (TPES) with respect to a PES is that 100% collection is easily achieved with a constant and excellent resolution, provided a tuneable light source is available, such as SR. With this method, we reported an ultimate electron threshold resolution under 1 meV with DELICIOUS II by using a very low extraction potential (V_{rep} = 5 V), and we have obtained the same performance with DELICIOUS III. Since this aspect was reported in detail, no further mention will be given here. Instead, we will focus on the performance of the electron divergent lens. As predicted by the raytracing simulations, the electron image magnification significantly improves the energy resolution of threshold photoelectrons, for a given extraction voltage. In Figure 3 are shown the Ar $(3p^{-1})$ $^2P_{3/2}$ threshold electrons images, recorded with a repeller of 250 V, without (Figure 3(a)) and with (Figure 3(b)) the use of the lens system, showing a magnification factor of about 3.4. The magnified image (Figure 3(b)) is slightly spatially shifted as compared to the non-magnified one. This effect is associated to the presence of stray fields in the interaction region, especially efficient for slow electrons, leading to some image distortion because of non-vanishing off-axis aberrations of the lens system. Such an effect becomes

Downloaded 30 May 2013 to 195.221.0.6. This article is copyrighted as indicated in the abstract. Reuse of AIP content is subject to the terms at: http://rsi.aip.org/about/rights_and_permissions

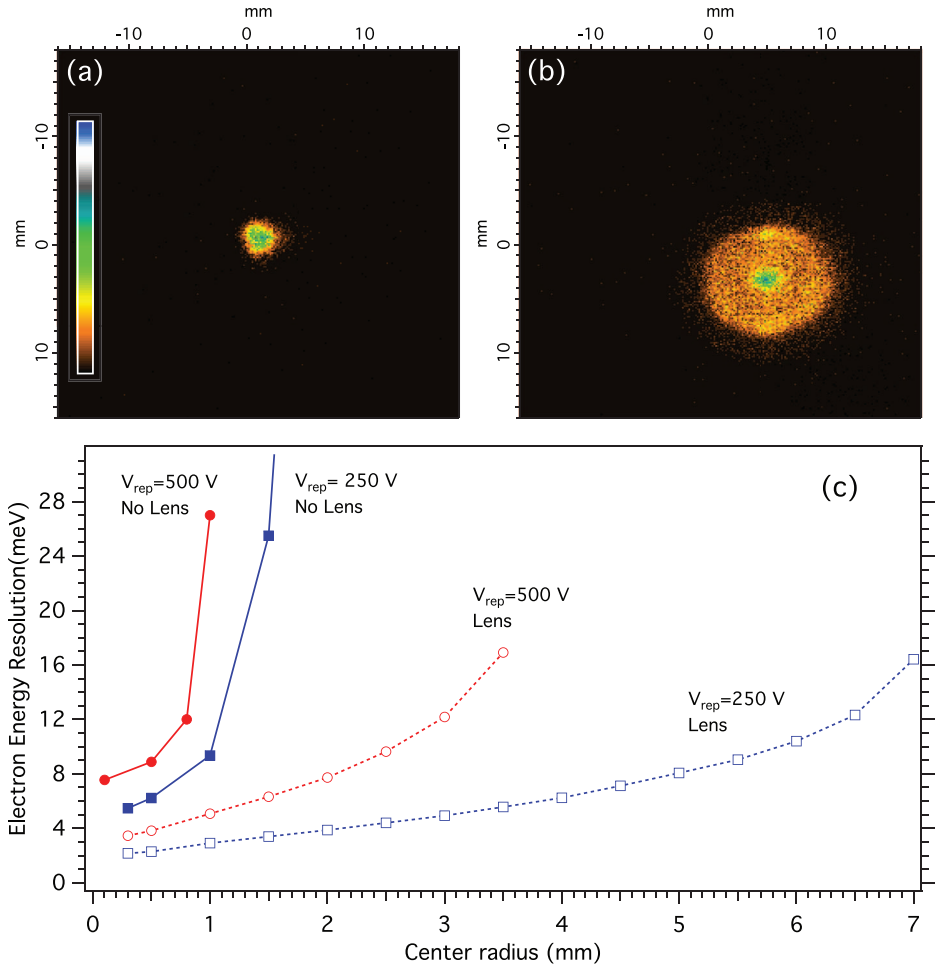

FIG. 3. Ar photoelectrons images obtained at a photon energy of 15.759 eV (KE_{ele} = 3 meV) and a repeller voltage of 250 V without (a) and with (b) the use of the magnifying lens system. (c) Threshold electron energy as a function of the radius of the central region used to collect slow electrons, for two different repeller voltages and lens configurations.

more important with decreasing repeller voltages, so that in practice one cannot use the lens below 50 V on the repeller. This limitation prevents us from improving the ultimate threshold electron resolution as compared to DELICIOUS II (∼0.8 meV).

However, a major feature of the lens is that it improves significantly the compromise between the threshold photoelectron and mass resolution, as shown in Figure 3(c), where it is demonstrated that, for a given repeller, the ultimate threshold electron resolution, i.e., for very small central zone radius, is improved by a factor of ∼2.3. In other words, since the electron resolution is proportional to the extraction field, it means that the resolution achieved with the use of the lens system is equivalent to that obtained with a repeller 2.3 times smaller without lens. As it will be clearly apparent in Secs. III B and III C, one of the main points is the improved corresponding ion mass resolution for a given electron resolution, i.e., the possibility to increase the repeller without losing in electron resolution thanks to the magnifying lens. It is important to say that, depending on the signal/resolution compromise desired, this gain can be further improved by increasing the central zone radius, as can be noted on the resolution curves in Figure 3(c).

B. Ion mass and kinetic energy resolution analysis

As mentioned in Sec. II A, the modified WM-TOF spectrometer includes an electrostatic lens to access the full 3D particle momentum distribution on the ion side so that the total ion kinetic energy is measured thorough the 2D particle's position on the PSD (E_{xy}) and its time of flight (E_z). The electrostactic lens can also be turned off by setting iL1 and iL2 to intermediate voltages so that the field in the second WM acceleration region is homogenous along the spectrometer axis, at the expense of losing the E_{xy} energy component. Thus, we distinguish between the two different modes of operation, lens on or off, and call them 3D momentum focusing and time focusing, respectively. Both modes, theoretically and experimentally, yield nearly identical mass resolutions, so that the only advantage of working in time focusing mode is to increase the lifetime of the ion detector when their energy information is not needed, since the particles are no longer focused on the detector plane.

The experimental mass resolution was measured with Xe due to its interesting natural isotope composition. In Figure 4 are illustrated the times of flight of Xe monomer (Figure 4(a)) and dimer (Figure 4(b)) obtained at 12.4 eV photon energy

Downloaded 30 May 2013 to 195.221.0.6. This article is copyrighted as indicated in the abstract. Reuse of AIP content is subject to the terms at: http://rsi.aip.org/about/rights_and_permissions

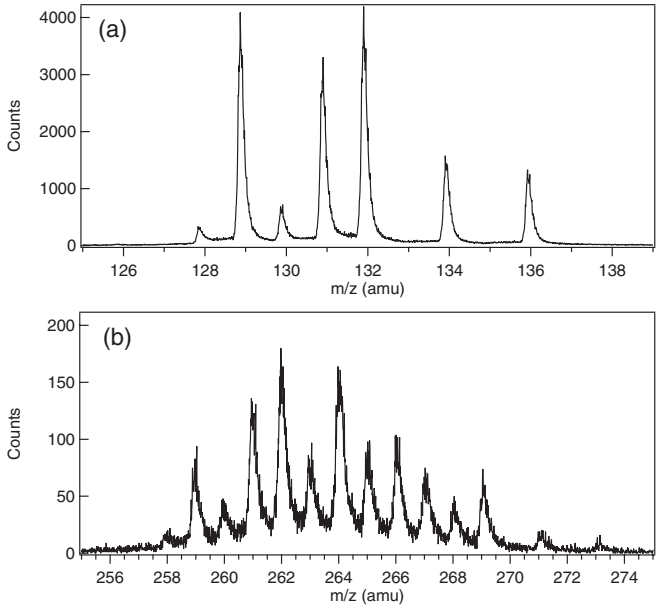

FIG. 4. (a) Xe and (b) Xe_2 time of flight recorded at 12.4 eV photon energy with a repeller of 500 V under the WM time focusing operation mode.

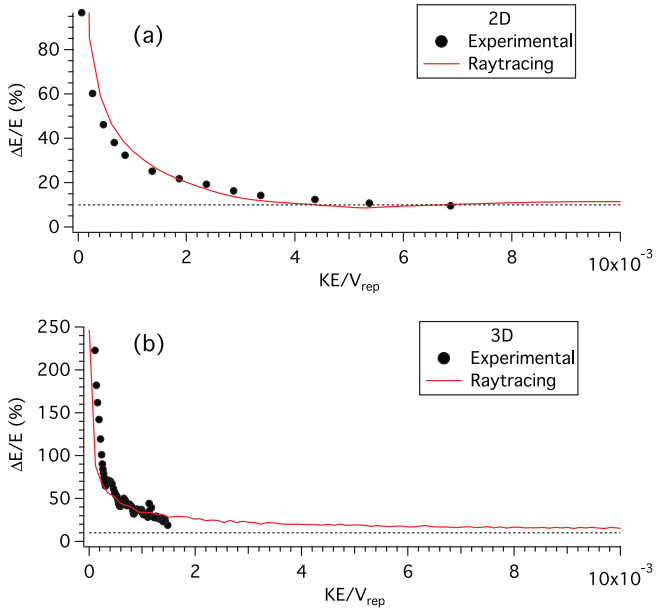

FIG. 5. (a) 2D ion kinetic energy resolution ΔE/E as a function of the E/V_{rep} ratio. Black solid circles represent the experimental values obtained at different ionization energies for Xe at a fixed repeller of 1000 V. (b) Full 3D ion kinetic energy resolution ΔE/E as a function of the E/V_{rep} ratio. Black solid circles represent the experimental values obtained from the N^+ correlation matrix in Figure 7(b). The red solid line corresponds to the simulated resolution assuming a cylindrical volume source of dimensions L = 6 mm and R = 100 μm. The horizontal dashed line at ΔE/E = 10% is shown as a visual aid.

in time focusing mode. We can observe that the resolution achieved is sufficient to separate all Xe dimer isotopes, albeit not fully. From the dimer peak widths, a precise value for the mass resolution—the maximum mass at which two adjacent masses can be perfectly separated, a requirement for using unambiguously the PEPICO scheme—can be extrapolated. In our case, this corresponds to $M_{max} = 250$ amu. If one considers that differentiation is achieved when two masses are separated by their FWHM, then the mass resolution reaches up to $M_{max} = 650$. Note that both values scale with $\sqrt{V_{rep}/E_z}$, and that we estimate the Xe_2 translational temperature along the z (detector) axis to be 40 K ($E_z = 3.4$ meV). Taking the full-peak separation value of $M_{max} = 250$ amu, this represents a gain of a factor of two with respect to the previous spectrometer.[4] For comparison purposes, we quote a mass resolving power of $M/\Delta M = 1600$ from Figure 4(a), for the m/z 132 Xe isotope. Although this value cannot be directly compared to the 900 reported by the NSRL group[7] due to the different extraction fields, geometries, and molecular beam conditions, we nevertheless note that their Xe TOF is qualitatively very similar to the one in Figure 4(a), despite of their longer ion flight path.

Regarding the ion kinetic energy, the WM-TOF has been calibrated both spatially (E_{xy}) and temporally (E_z) in the 3D momentum focusing mode, and its performance determined.

The 2D kinetic energy distribution (E_{xy}) characterization was performed using the same procedure as on the electron side. After inversion of the electrodes' polarity, we recorded Xe photoelectrons images on the ion side at several photon energies for a given extraction voltage. The corresponding C coefficient obtained for the ion side for the present geometry is $C_{WM} = 20$ cm. The 2D resolution curve, extracted from the rare gas photoelectron images, as a function of ρ is displayed in Figure 5(a), showing an excellent agreement with the raytracing simulation. Because the WM electrostatic lens is outside of the interaction region, the resolution is somewhat degraded with respect to the VMI, reaching down to ΔE/E = 10% at the detector's edge.

The relation between the kinetic energy along the detector's axis and the TOF is well known for a WM spectrometer, when the extraction field is homogeneous:

$$E_z = \frac{(q\varepsilon\Delta T)^2}{2M},$$

where q is the particle charge, ε is the extraction electric field, M is the mass of the ion, and $\Delta T = t_0 - TOF$, where t_0 is the particle's TOF when $E_z = 0$. Although the VMI's extraction field is not homogenous, we can define an effective field ε inside the extraction region of a VMI, which is given by

$$\varepsilon = \frac{V_{rep}(1-r)\alpha}{d},$$

where d is the distance between the repeller and extractor electrodes, V_{rep} is the repeller voltage, $r = V_{ext}/V_{rep}$ is the VMI magic ratio, and α is a coefficient accounting for the leak of the electric field through the extractor and towards the drift electrode. Only one coefficient, α, is then needed to obtain the E_z vs ΔT relation. An experimental $\alpha = 1.38603$ was found by using a well-known system such as the N^+ fragment from the photodissociation of N_2 at 25.6 eV through the $C^2\Sigma_u^+$ state (see Sec. III C). The experimental value differs from the calculated by less than 2% ($\alpha = 1.36319$).

The ion kinetic energy resolution in full 3D mode is plotted in Figure 5(b) alongside the raytracing predictions. Once again, the agreement between the simulated and measured values is remarkable. Although in this case the experimental data do not cover the entire detector range, we have reached

Downloaded 30 May 2013 to 195.221.0.6. This article is copyrighted as indicated in the abstract. Reuse of AIP content is subject to the terms at: http://rsi.aip.org/about/rights_and_permissions

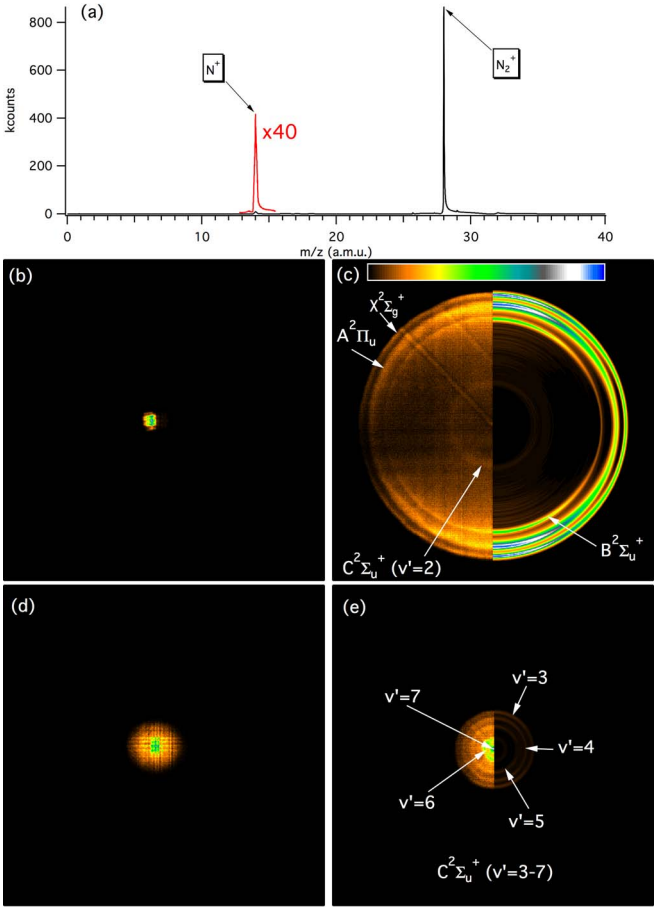

FIG. 6. Photoionization of N_2 at hv = 25.1 eV obtained with 1750 V on the repeller plate. (a) Ion mass spectrum; (b) and (c) ion and electron images corresponding to m/z = 28; (d) and (e) ion and electron images corresponding to m/z = 14. The light's electric vector is parallel to the north/south axis in the photoelectron images. The left-hand side of the photoelectron images corresponds to the raw data, while the right is the output from the pBasex inversion algorithm.

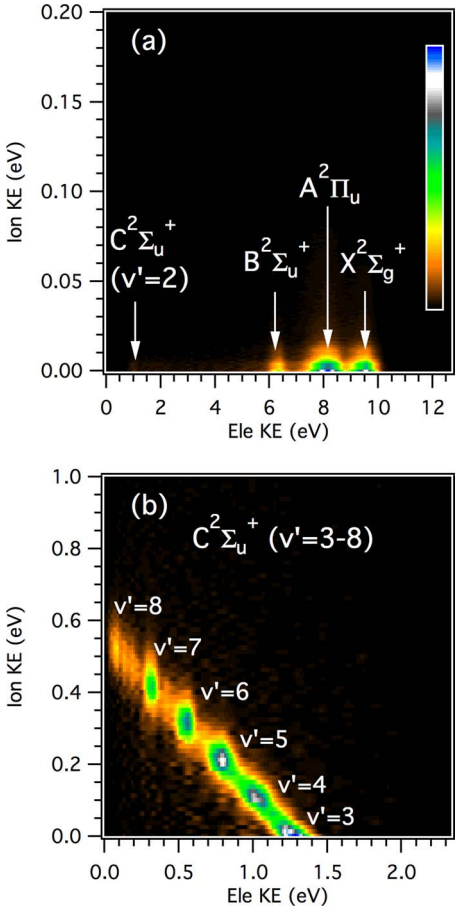

FIG. 7. (a) Electron/ion kinetic energy correlation diagram of N_2^+ obtained at hv = 25.1 eV with 1750 V on the repeller. The arrows point to the different non-dissociative states of N_2^+. (b) Same for the N^+ fragment at hv = 25.6 eV where an experimental zoom of the C state was performed by lowering the potential on the repeller to 300 V. The image illustrates the pre-dissociation process of the different vibrational states from $v' = 3$ to 8 of the C state.

a value of $\Delta E/E = 19\%$ which, in view of the accordance with the simulations, can readily be extrapolated to an ultimate value of 15% at the detector's edge. Note that the curve shown in Figure 5(b) is independent of the ion mass or repeller, because the 120 ps temporal resolution of the TDC is not a limiting factor for the narrower TOF profiles expected at lighter masses or higher repeller voltages.

C. Coincidence mode

1. Photoionization of N_2

To illustrate the coincidence mode of operation we have chosen the N_2 molecule, whose photoionization spectra in the first dissociative ionization region are well known.[31,32] We have chosen an ionization energy of 25.1 eV, above the first dissociative channel leading to $N^+(^3P) + N(^4S)$, which opens at 24.29 eV. This fragmentation pathway can be accessed via the bound cation state $C^2\Sigma_u^+$ through spin-orbit coupling with the quartet $f^4\Pi_u$ state.[33,34] Thus, the $C^2\Sigma_u^+$ state will correlate to the N^+ fragment, while the rest of the accessible states lying below 25.1 eV will lead only to N_2^+. Figure 6 shows the electron and ion images correlated with the m/z = 14 and 28 masses. As expected, the photoelectrons linked to the N_2^+ correspond to the non-dissociative states $X^2\Sigma_g^+$, $A^2\Pi_u$, $B^2\Sigma_u^+$, and to $C^2\Sigma_u^+(v = 2)$, which lies below the first dissociation limit. Note that the ionization cross-sections for the $C^2\Sigma_u^+(v = 0,1)$ states are significantly weaker than for the $C^2\Sigma_u^+(v = 2)$[31] and thus are not observed here. On the other hand, the photoelectrons correlated to the N^+ fragment correspond to the $v = 3$–7 vibrational states of $C^2\Sigma_u^+$ which predissociate via spin-orbit coupling to the $f^4\Pi_u$ state. Looking at the photoion images, it is clear that, since they are formed by photodissociation, the N^+ ion possesses a much higher kinetic energy than the parent N_2^+, which only has the low translational temperature of the molecular beam.

For a more detailed view, a kinetic energy correlation diagram is displayed in Figure 7 for the N^+ and N_2^+ ions. Figure 7(b) has been recorded at a slightly higher photon energy (hv = 25.6 eV) and a lower extraction field for a better definition of the ion kinetic energy. The diagram plots the intensity as a function of ion kinetic energy—as derived from the 3D momentum obtained from the (x,y) PSD position and the TOF (z)—and electron kinetic energy, obtained by Abel inversion of the image.[28] For the N_2^+, only cold ions exist and thus, all the photoelectron energies correlate to close-to-

Downloaded 30 May 2013 to 195.221.0.6. This article is copyrighted as indicated in the abstract. Reuse of AIP content is subject to the terms at: http://rsi.aip.org/about/rights_and_permissions

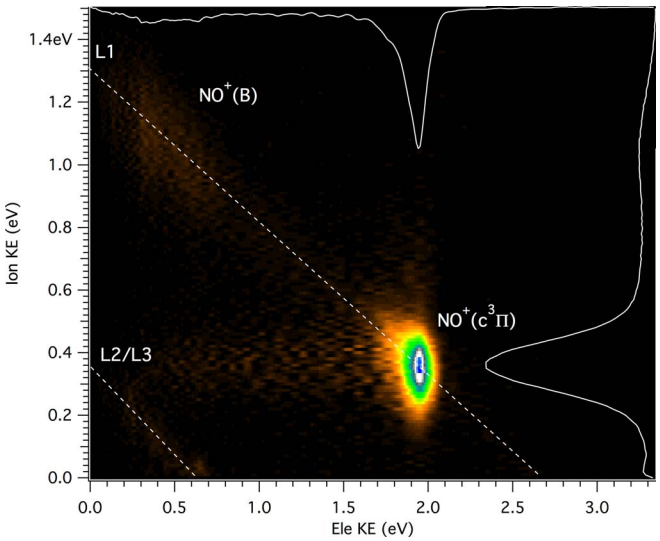

FIG. 8. (a) Electron/ion kinetic energy correlation diagram of the N^+ fragment from NO dissociative ionization obtained at hν = 23.65 eV with 500 V on the repeller. The dashed white lines represent the dissociation limits. L1 can be reached from both B and c states of NO^+. The solid white lines correspond to the horizontal and vertical matrix projections. (b) N^+ recoil distribution for dissociation via the c state (Process I in the text). The light's electric vector is parallel to the x axis while the detector plane is perpendicular to the z axis.

zero ion energies. More interesting is the N^+ diagram, where the different round spots observed correspond to each of the different pre-dissociation pathways leading to the first dissociation limit, according to the energy conservation expression $[IE(C^2\Sigma_u{}^+, \nu_i) - D1] \times 0.5 = h\nu - KE_{ele}$, where IE is the ionization energy of the ith vibrational state (i = 3–8), D1 is the first dissociation limit at 24.29 eV, hν is 25.6 eV, and KE_{ele} is the photoelectron kinetic energy. The factor 0.5 on the left-hand side is present since the neutral N atom produced in the fragmentation alongside the N^+, takes half of the translational energy.

2. Photoionization of NO

For performance comparison purposes, the photoionization of NO at hν = 23.65 eV was also recorded, since it has been comprehensively studied by Dowek *et al.*[35,36] with a double 3D momentum imaging technique. At this energy, the main dissociation channel, named Process I, is

$$NO(X^2\Pi) + h\nu \rightarrow NO^+(c^3\Pi) + e^- \rightarrow N^+(^3P) + O(^3P) + e^-.$$

The corresponding electron/ion kinetic energy correlation diagram for the N^+ fragment is presented in Figure 8(a). The image shows the main dissociation channel, Process I, leading to a mean ion KE_{N^+} of 0.36 eV (center of mass KE of 0.88 eV), and a mean electron KE_{ele} of 1.94 eV, in agreement with previously reported values.[35] There is a weak signal, barely visible in Figure 8(a), corresponding to $KE_{N^+} \approx 1.13$ eV and $KE_{ele} \approx 0.39$ eV which is assigned to the L1 limit attained via the $NO^+(B)$ state,[36] plus two more dissociation limits L2/L3. A qualitative comparison with the correlation diagram obtained by Dowek *et al.* (Figure 5(a) of Ref. 36) shows that for a similar electron bandwidth, the electron resolution of DELICIOUS III is far superior. A projection on the electron KE of Figure 8(a) gives a FWHM of 0.14 eV at 1.94 eV, an estimated four times better than with the technique used by Dowek *et al.*,[36] highlighting the advantage of a VMI with respect to an imaging device, which is limited by both the spatial resolution and the uncertainty of the electron's TOF measurement, quickly degraded for increasingly fast electrons. Concerning the ions, the projection of Figure 8(a) on the ion KE, gives a FWHM of 0.18 eV at 0.36 eV. Interestingly, our ion spectrometer also performs much better than the ion analyzer used by Dowek *et al.*,[36] even though it is based on the same principle.

If we now select only Process I, we can readily obtain the ion recoil angular distribution since both the position and timing information are available for the ion. The raw angular distribution recorded for the N^+ fragment produced via Process I is shown in Figure 8(b). If this distribution is fitted with the well-known Legendre expansion,[37] an anisotropy parameter of $\beta = 1.0$ is found, exactly the same as previously reported.[13] Because the 3D momentum of each individual ion is recorded, DELICIOUS III can provide the photoelectron images filtered for a given ion recoil direction which, in the case of the diatomic NO where the fragmentation via Process I is fast, defines the molecular orientation at the time of photoionization. Hence, the photoelectron images can be converted into Molecular Frame Photoelectron Angular Distributions or MF-PADs. However, and this constitutes the main disadvantage of VMI spectrometers over COLTRIMS-type techniques, the fact that the photoelectron images do not provide the velocity component perpendicular to the detector plane, heavily restricts the situations where the MF-PADs can be fully retrieved. Indeed, the treatment of VMI images by Abel inversion requires that the 3D photoelectron cloud have an axis of symmetry contained into the image plane, so that one of the 3 dimensions is made redundant and the reconstructed 2D image contains all the information. For example, in the case of the photoionization of NO with circularly polarized light, this is only possible when the molecular axis is parallel to the light's electric vector,[35] while all the other orientations are only accessible through the full 3D measurement of the photoelectron velocity vector.

In view of the above, we attempted to use the single-bunch pulsed mode of operation of the synchrotron SOLEIL, available one week per semester, providing light pulses of 70 ps duration (FWHM) separated by 1176 ns. Thus, the electron TOF could be experimentally measured with respect to the light pulse to obtain the missing third dimension. Unfortunately, we found that the electron TOF and the kinetic energy along the detection axis were completely uncorrelated, rendering the temporal slicing of the electrons impossible, even at low extraction fields. Since electron slicing with a VMI has already been achieved successfully,[17] we conclude that our failed attempt can be attributed to the electronics chain before the TDC (signal decoupling from the MCP, plus preamplifier, and discriminator), and possibly to our much larger light pulse duration.

However, although a full 3D vector correlation is not possible with our setup, we can measure in the multi-bunch mode

Downloaded 30 May 2013 to 195.221.0.6. This article is copyrighted as indicated in the abstract. Reuse of AIP content is subject to the terms at: http://rsi.aip.org/about/rights_and_permissions

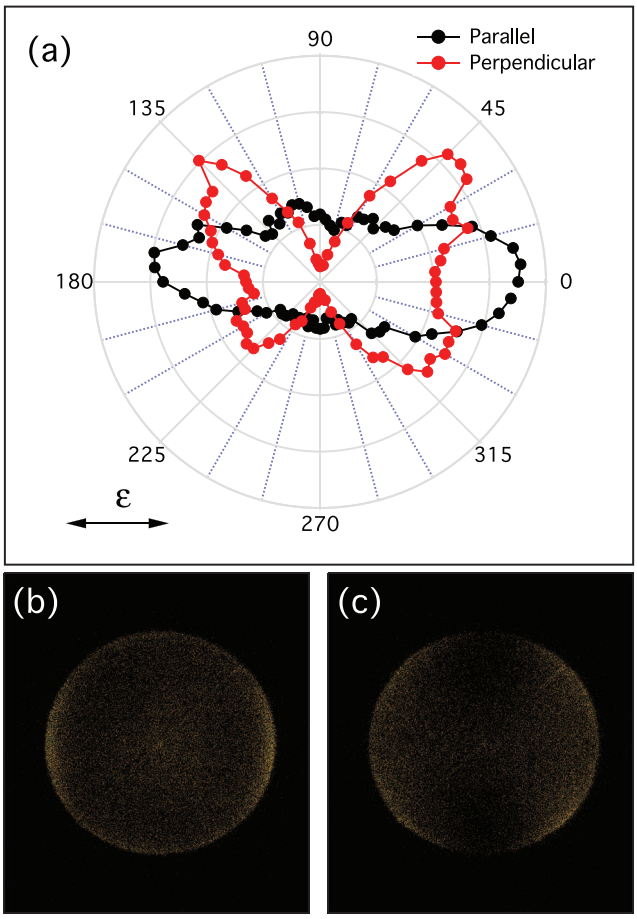

FIG. 9. (a) Polar θ_e plot of NO PADs from Process I obtained at hν = 23.65 eV for two different NO orientations, parallel (black circles, $0 \leq \theta_i \leq 20°$ and $160 \leq \theta_i \leq 180°$) and perpendicular (red circles, $80 \leq \theta_i \leq 100°$) to the light electric field vector (ε). The polar intensities have been obtained by onion peeling[14] of the corresponding photoelectron images—(b) parallel; (c) perpendicular—and integration over $\Delta\theta_e = 5°$. The black and red lines are shown just for guidance. The double arrow defines the light's electric vector. Note that the small asymmetry along the light's polarization axis is due to the inhomogeneous response of the MCPs.

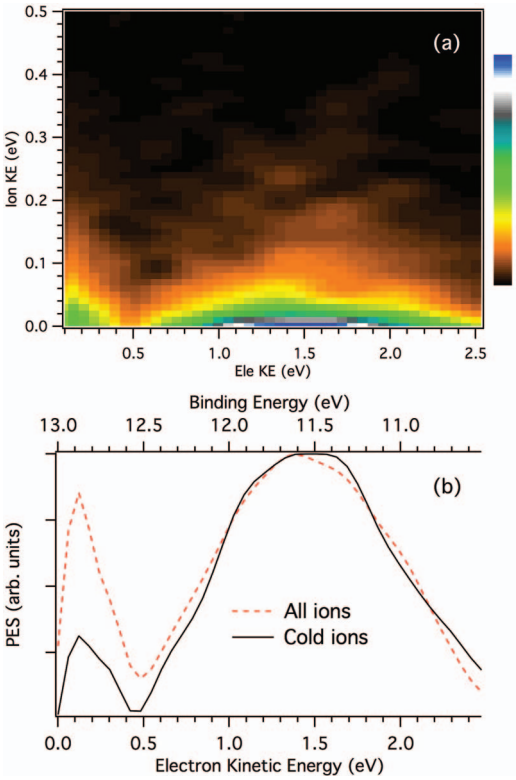

FIG. 10. (a) Electron/ion kinetic energy correlation diagram of the CF_3^+ fragment obtained at hν = 13.0 eV with 500 V on the repeller. (b) Derived PESs for all fragment kinetic energies (red dashed line) and only those having translational energies in the 0–5 meV range (black solid line).

the projection of the electron's momentum onto the detector plane, so that the electron angular distribution will be averaged over the laboratory frame azimuthal angle ϕ_e, and correlate it with the N^+ ion's direction, as has already been done for inner-shell excited BF_3.[38] This has been done for Process I using linearly polarized light, and the results are shown in Figure 9 in the form of electron polar plots for two different orientations of the NO molecule—defined by the N^+ direction of ejection according to the fast recoil approximation—parallel and perpendicular, with respect to the light's polarization axis. The PADs exhibit a strong anisotropy that changes dramatically with the orientation of the molecular axis, as originally demonstrated by Lafosse *et al.*[13] with similar results.

3. Photoionization of CF_3 radical

We have recently studied the photoelectron spectroscopy of the $CF_3^\bullet$ radical produced by the incomplete flash pyrolysis of C_2F_6.[10] In this study, the energy range was limited by the dissociative ionization of the precursor which was determined to be around 12.3 eV for the production of CF_3^+ fragment. Beyond this high limit, it was impossible with our previous spectrometer to obtain the electron spectroscopy of pure $CF_3^\bullet$ radical, since the m/z = 69 mass would be contaminated by the CF_3^+ fragment coming from $C_2F_6^+$. However, with DELICIOUS III the two processes, direct and dissociative ionization, leading to the same mass in the ion TOF can be disentangled via the ion kinetic energy release. Therefore, in order to test these new capabilities, we decided to rapidly revisit the photoionization of this radical at the fixed photon energy of 13 eV, where we had roughly estimated that 40% of the signal on m/z 69 was due to the dissociative ionization of the precursor.

Figure 10(a) shows the kinetic energy correlation diagram for the CF_3^+ fragment, acquired over 15 min. Projection of the total intensity along the electron KE axis provides the PES in Figure 10(b), corresponding to the ionization of both $CF_3^\bullet$ and the remaining non-pyrolyzed precursor C_2F_6. The signal above 12.5 eV binding energy belongs to a dissociative state of $C_2F_6^+$, while the large band with a maximum around 11.5 eV is assigned to the ground state of the radical cation,[10] which shows a long progression on the umbrella bending mode due to a large geometry change between neutral and ionic CF_3, starting at 9.0 eV and vanishing at around 12.5 eV binding energy.

Since the CF_3^+ cation formed by direct ionization of the radical will have a smaller translational energy, the PES

Downloaded 30 May 2013 to 195.221.0.6. This article is copyrighted as indicated in the abstract. Reuse of AIP content is subject to the terms at: http://rsi.aip.org/about/rights_and_permissions

correlated to the cold ions should belong solely to the radical. Figure 10(b) also displays the PES from CF_3^+ ions having translational energies between 0 and 5 meV. It is clear that the contribution to the total electron signal of the region assigned to the dissociative ionization (hv > 12.5 eV) has now been reduced from around 18% to 11%, although it has not completely disappeared. The remaining signal could arise from the presence of an excited state of the CF_3^+, although theoretically, the first excited state ($^3A_2$) of the CF_3^+ cation is not expected until $h\nu = 15.85$ eV.[39] However, Lifshitz and Chupka[40] measured the PES of CF_3 radical using a different precursor (CF_3CH_2ONO), and found that the signal increased above 12.4 eV although, unfortunately, the presence of an excited state cannot be confirmed since their PES stops soon after, at 12.5 eV.

IV. CONCLUSION

We have presented the double imaging coincidence spectrometer DELICIOUS III, which, since February 2012, is installed in one of the permanent endstations of the DESIRS beamline and thus available to the gas phase user community, with typically seven projects performed per semester with this set-up. The electron analyzer is based upon the VMI principle and provides an ultimate resolution for fast electrons below 5%, and a constant absolute ultimate resolution of ~1 meV in the threshold electron mode. For the latter mode, an Einzel lens with a magnification factor of 3.4 greatly improves the resolution for a given extraction field due to the increased fast electron discrimination. This improvement is, at the very least, a factor of 2.3 and can reach much higher values depending on the chosen signal/resolution compromise in the TPES treatment. This means that higher extraction fields can now be applied to reach the same electron resolution, with a positive impact on the ion mass/electron resolution compromise. In addition, the bandwidth has now been multiplied by a factor of 3.6 with respect to its predecessor, DELICIOUS II, by moving to a 80 mm delay-line anode PSD. Furthermore, a double skimmer chamber will be installed on the SAPHIRS permanent endstation in the imminent future to improve the electron and ion energy resolution by reducing the length of the cylindrical volume source.

The ion analyzer consists of a modified WM capable of providing a good spatial resolution (down to 10%) and full 3D kinetic energy resolution (15%) without compromising the ion mass resolution, which has now doubled to reach a value of ~250 amu. The measurement of the complete velocity vector provides the ion's translational energy and angular distributions so that the photoelectrons images can be filtered with coincident ions in terms of mass, energy, and ion recoil direction, opening new and exciting research avenues, notably in photochemistry or clusters science.

ACKNOWLEDGMENTS

We are indebted to Jean-François Gil for his crucial role on the mechanical design and assembly of DELICIOUS III. We also thank Robert Sellem and David Heurteau from the DTPI for helpful discussions concerning the data acquisition chain, and for the development of the TDC-V4. Finally, we warmly thank the SOLEIL staff for smoothly running the facility.

[1] A. G. Suits and R. E. Continetti, *Imaging in Chemical Dynamics* (American Chemical Society, Washington, D.C., 2000).
[2] K. L. Reid, Mol. Phys. **110**(3), 131 (2012).
[3] A. T. J. B. Eppink and D. H. Parker, Rev. Sci. Instrum. **68**(9), 3477 (1997).
[4] G. A. Garcia, H. Soldi-Lose, and L. Nahon, Rev. Sci. Instrum. **80**(2), 023102 (2009).
[5] L. Nahon, N. de Oliveira, G. A. Garcia, J.-F. Gil, B. Pilette, O. Marcouillé, B. Lagarde, and F. Polack, J. Synchrotron Radiat. **19**(4), 508 (2012).
[6] A. Bodi, M. Johnson, T. Gerber, Z. Gengeliczki, B. Sztaray, and T. Baer, Rev. Sci. Instrum. **80**(3), 034101 (2009).
[7] X. Tang, X. Zhou, M. Niu, S. Liu, J. Sun, X. Shan, F. Liu, and L. Sheng, Rev. Sci. Instrum. **80**(11), 113101 (2009).
[8] P. O'Keeffe, P. Bolognesi, M. Coreno, A. Moise, R. Richter, G. Cautero, L. Stebel, R. Sergo, L. Pravica, Y. Ovcharenko, and L. Avaldi, Rev. Sci. Instrum. **82**(3), 033109 (2011).
[9] B. Gans, L. A. V. Mendes, S. Boyé-Péronne, S. Douin, G. Garcia, H. Soldi-Lose, B. K. Cunha de Miranda, C. Alcaraz, N. Carrasco, P. Pernot, and D. Gauyacq, J. Phys. Chem. A **114**(9), 3237 (2010).
[10] H. Dossmann, G. A. Garcia, L. Nahon, B. K. C. de Miranda, and C. Alcaraz, J. Chem. Phys. **136**(20), 204304 (2012).
[11] B. Gans, G. A. Garcia, S. Boyé-Péronne, J.-C. Loison, S. Douin, F. Gaie-Levrel, and D. Gauyacq, J. Phys. Chem. A **115**(21), 5387 (2011).
[12] W. C. Wiley and I. H. Maclaren, Rev. Sci. Instrum. **26**, 1150 (1955).
[13] A. Lafosse, M. Lebech, J. C. Brenot, P. M. Guyon, O. Jagutzki, L. Spielberger, M. Vervloet, J. C. Houver, and D. Dowek, Phys. Rev. Lett. **84**(26), 5987 (2000).
[14] C. Bordas, F. Paulig, H. Helm, and D. L. Huestis, Rev. Sci. Instrum. **67**(6), 2257 (1996).
[15] D. Dowek, J. C. Brenot, P. M. Guyon, J. C. Houver, A. Lafosse, M. Lebech, O. Jagutzki, and L. Spielberger, Nucl. Instrum. Methods Phys. Res. A **477**(1–3), 323 (2002).
[16] J. Ullrich, R. Moshammer, A. Dorn, R. Dorner, L. P. H. Schmidt, and H. Schniidt-Bocking, Rep. Prog. Phys. **66**, 1463 (2003).
[17] A. Vredenborg, W. G. Roeterdink, and M. H. M. Janssen, Rev. Sci. Instrum. **79**(6), 063108 (2008).
[18] A. Vredenborg, C. S. Lehmann, D. Irimia, W. G. Roeterdink, and M. H. M. Janssen, ChemPhysChem **12**(8), 1459 (2011).
[19] C. S. Lehmann, N. B. Ram and M. H. M. Janssen, Rev. Sci. Instrum. **83**(9), 093103 (2012).
[20] A. Bodi, P. Hemberger, T. Gerber, and B. Sztaray, Rev. Sci. Instrum. **83**(8), 083105 (2012).
[21] K. Hosaka, J.-i. Adachi, A. V. Golovin, M. Takahashi, N. Watanabe, and A. Yagishita, Jpn. J. Appl. Phys. **45**(3A), 1841 (2006).
[22] G. Prumper and K. Ueda, Nucl. Instrum. Methods Phys. Res. A **574**(2), 350 (2007).
[23] D. Ceolin, G. Chaplier, M. Lemonnier, G. A. Garcia, C. Miron, L. Nahon, M. Simon, N. Leclercq, and P. Morin, Rev. Sci. Instrum. **76**(4), 043302 (2005).
[24] M. Lebech, J. C. Houver, and D. Dowek, Rev. Sci. Instrum. **73**(4), 1866 (2002).
[25] H. L. Offerhaus, C. Nicole, F. Lepine, C. Bordas, F. Rosca-Pruna, and M. J. J. Vrakking, Rev. Sci. Instrum. **72**(8), 3245 (2001).
[26] A. Bodi, B. Sztaray, T. Baer, M. Johnson, and T. Gerber, Rev. Sci. Instrum. **78**(8), 084102 (2007).
[27] G. A. Garcia, L. Nahon, C. J. Harding, E. A. Mikajlo, and I. Powis, Rev. Sci. Instrum. **76**(5), 053302 (2005).
[28] G. A. Garcia, L. Nahon, and I. Powis, Rev. Sci. Instrum. **75**(11), 4989 (2004).
[29] M. J. Verheijen, H. C. W. Beijerinck, W. A. Renes, and N. F. Verster, J. Phys. E: Sci. Instrum. **17**(12), 1207 (1984).
[30] B. Sztaray and T. Baer, Rev. Sci. Instrum. **74**(8), 3763 (2003).
[31] H. Yoshii, T. Tanaka, Y. Morioka, T. Hayaishi, and R. I. Hall, J. Mol. Spectrosc. **186**(1), 155 (1997).
[32] C. Nicolas, C. Alcaraz, R. Thissen, M. Vervloet, and O. Dutuit, J. Phys. B **36**(11), 2239 (2003).
[33] M. Hochlaf, G. Chambaud, and P. Rosmus, J. Phys. B **31**(17), 4059 (1998).

Downloaded 30 May 2013 to 195.221.0.6. This article is copyrighted as indicated in the abstract. Reuse of AIP content is subject to the terms at: http://rsi.aip.org/about/rights_and_permissions

[34]M. Hochlaf, G. Chambaud, and P. Rosmus, J. Phys. B **30**(20), 4509 (1997).
[35]M. Lebech, J. C. Houver, A. Lafosse, D. Dowek, C. Alcaraz, L. Nahon, and R. R. Lucchese, J. Chem. Phys. **118**(21), 9653 (2003).
[36]D. Dowek, M. Lebech, J. C. Houver, and R. R. Lucchese, Mol. Phys. **105**(11–12), 1757 (2007).
[37]S. Yang and R. Bersohn, J. Chem. Phys. **61**, 4400 (1974).
[38]T. Mizuno, J. Adachi, M. Kazama, M. Stener, P. Decleva, and A. Yagishita, Phys. Rev. Lett. **110**(4), 043001 (2013).
[39]C. Larrieu, M. Chaillet, and A. Dargelos, J. Chem. Phys. **96**(5), 3732 (1992).
[40]C. Lifshitz and W. A. Chupka, J. Chem. Phys. **47**, 3439 (1967).

Downloaded 30 May 2013 to 195.221.0.6. This article is copyrighted as indicated in the abstract. Reuse of AIP content is subject to the terms at: http://rsi.aip.org/about/rights_and_permissions